



1 **Odds and ends of atmospheric mercury in Europe and over northern Atlantic Ocean: Tem-**
2 **poral trends of 25 years of measurements.**

3
4 Danilo Custódio^{1*}, Franz Slemr², Katrine Aspömpfer³, T. Gerard Spain⁴, Fidel F. Pankratov⁵, Iana
5 Strigunova^{6, a}, Kokeitso Molepo¹, Henrik Skov⁷, Johannes Bieser¹, Ralf Ebinghaus¹.

6
7 ¹ Helmholtz-Zentrum Hereon, Institute of Coastal Research, Max-Planck-Str. 1, D-21502 Geesthacht, Germany.

8 ² Max Planck Institute for Chemistry, Mainz, Germany.

9 ³ NILU – Norwegian Institute for Air Research, Kjeller, Norway.

10 ⁴ National University of Ireland, Galway, Ireland.

11 ⁵ Institute of Northern Environmental Problems, Kola Science Center, Russian Academy of Sciences, Fersman Str. 14A, Apatity, 184200,
12 Russia.

13 ⁶ Meteorological Institute, MI, Universität Hamburg, Hamburg, Germany.

14 ⁷ Department of Environmental Science, iClimate, Aarhus University, Frederiksborgvej 399, 4000 Roskilde, Denmark

15 ^a International Max Planck Research School on Earth System Modelling, Hamburg, Germany.

16 * Correspondence to: Danilo Custodio (danilo.custodio@hereon.de)

17
18 Manuscript aim:

19 To determine the atmospheric mercury trend on a continental scale and evaluate the driving factor
20 of the downward trend in mercury in the Northern Atlantic and Europe. Also, to assess the time
21 variability in the light of atmospheric transport patterns, and regional sources.

22
23
24 **Abstract**

25 The Global Monitoring Plan of the Minamata Convention on Mercury was established to generate long-term
26 data necessary for evaluating the effectiveness of regulatory measures at a global scale. After 25 years
27 monitoring (since 1995), Mace Head is one of the atmospheric monitoring stations with the longest mercury
28 record, and has produced sufficient data for the analysis of temporal trends of Total Gaseous Mercury (TGM)
29 in Europe and the Northern Atlantic. Using concentration-weighted trajectories for atmospheric mercury
30 measured at Mace Head as well as other five locations in Europe, Amderma, Andøya, Villum, Waldhof and
31 Zeppelin we identify the regional probabilistic source contribution factor and its changes for the period of
32 1996 to 2019.

33 Temporal trends indicate that concentrations of mercury in the atmosphere in Europe and the Northern
34 Atlantic have declined significantly over the past 25 years, at a non-monotonic rate averaging of 0.03 ng m^{-3}
35 year^{-1} . Concentrations of TGM at remote marine sites were shown to be affected by continental long-range
36 transport, and evaluation of reanalysis back-trajectories display a significant decrease of TGM in continental
37 air masses from Europe in the last two decades. In addition, using the relationship between mercury and
38 other atmospheric trace gases that could serve as a source signature, we perform factorization regression
39 analysis, based on positive rotatable factorization of non-singular matrix to solve probabilistic mass function.
40 We reconstructed atmospheric mercury concentration and assessed the contribution of the major natural



41 and anthropogenic sources. The positive matrix factorization (PMF) reveals that the downward trend is
42 mainly associated with a factor with a high load of long-lived anthropogenic species.

43
44

45 **1 Introduction**

46 Mercury is a toxic pollutant of crucial concern to public health globally. Due to its neurotoxicity,
47 bioaccumulation, and long-range atmospheric transport, mercury was added to the priority list of several
48 international agreements and conventions dealing with environmental protection, including the Minamata
49 Convention on Mercury (e.g. Driscoll et al., 2013). Following the entry-into-force of the Stockholm Convention
50 (SC) in 2004 accompanied by the Minamata convention in 2013 to restrict releases of mercury and its
51 compounds to the environment, a Global Monitoring Plan was devised to evaluate the effectiveness of
52 regulatory measures at regional and global scales. At this time, regions such as Western Europe and North
53 America have already established monitoring networks for mercury in air and precipitation some of which
54 have been in operation since the 1990s (Schmeltz et al., 2011; Gay et al., 2013; EMEP, 2020; www.gmos.eu;
55 www.gos4m.org).

56

57 During the past decades, atmospheric mercury concentrations in the Northern Hemisphere decreased
58 substantially (Slemr et al., 2003; Cole et al., 2014; Steffen et al., 2015; Weigelt et al., 2015; Weiss-Penzias et
59 al. 2016; Marumoto et al., 2019; Custodio et al. 2020). This downward trend has been attributed to
60 decreasing emissions from the North Atlantic Ocean due to decreasing mercury concentrations in subsurface
61 water (Soerensen et al., 2012) and more recently to decreasing global anthropogenic emissions mainly due
62 to the decline of mercury release from commercial products (Horowitz et al., 2014) and the changes of
63 $\text{Hg}^0/\text{Hg}^{2+}$ speciation in flue gas of coal-fired utilities after implementation of NO_x and SO₂ emission controls
64 (Zhang et al., 2016). Mercury uptake by terrestrial vegetation has also been recently proposed as a
65 contributor to the downward trend (Jiskra et al., 2018).

66

67 In a 5-year source apportionment study, Custodio et al. (2020) show that a factor with high load of long lived
68 anthropogenic atmospheric species could explain the decrease of TGM at Mace Head. This decrease is
69 consistent with a decrease in the anthropogenic mercury emissions inventory in Europe and North America
70 (Horowitz et al. 2014). Wu et al., (2016) estimated that China's emissions also decreased since 2012 which
71 could have a hemispheric effect. However, the downward trend of global anthropogenic mercury emissions
72 needs to be confirmed by atmospheric observations, and a long-term evaluation of the time series of still not
73 unknown sources and its implication should be assessed.

74 This study reports continuous long-term temporal trends of TGM in the Northern Atlantic, Arctic, and Europe,
75 reporting mercury atmospheric concentrations at Mace Head (1995-2019), Amderma 2001-2017), Andøya



76 (2010-2019), Villum (1999-2019), Waldhof (2005-2019), and Zeppelin (2000-2019). Here, we combine a long-
77 time series of atmospheric mercury observed at these sites with calculated 120-hour reanalysis backward
78 trajectories in order to investigate transport and long-term changes in concentration patterns on the regional
79 scale.

80 On this raw, this paper aims to evaluate the TGM trend on a continental scale and the contribution of the
81 baseline factor as a driver of the downward trend in mercury for the Northern Atlantic and Europe.

82 Based on long-range Lagrangian reanalysis backward trajectories and receptor-modelling, we investigate the
83 trends and sources of mercury in the atmosphere, assessing the inter-annual variability on the light of
84 atmospheric transport patterns and changes in the regional emissions. In addition, we exploit atmospheric
85 mercury temporal variability, which can be used as additional constraints to improve the ability of models to
86 predict the cycling of mercury in the atmosphere.

87

88 2 Experimental

89

90 • Sampling sites

91

92 Data from six sites in Europe and Greenland with the longest records of atmospheric mercury concentrations
93 were selected for this study: Mace Head (data available 1995 – 2019), Zeppelin (2000 – 2019), Waldhof (2006
94 – 2019), Villum (2008 – 2019), Andøya (2010 -2019), and Amderma (2001 – 2013). Mace Head and Waldhof
95 are mid-latitude stations, Zeppelin, Amderma, and Villum can be classified as Arctic ones. Andøya, though at
96 latitude comparable to that of Amderma, is behaves more like a mid-latitude station because the ocean
97 around it is ice free for most of the year.

98

99 The Mace Head Global Atmosphere Watch (GAW) Station (53°20` N and 9°32W, 8 m above sea level; air-
100 sampling inlet 18 m a.s.l.) is located on the west coast of Ireland on the shore of the North Atlantic Ocean,
101 offering ideal conditions to evaluate both natural and anthropogenic pollutants in oceanic and continental
102 air masses as described by Stanley et al. (2018). The station was part of the GMOS network and mercury
103 measurements are described in detail by Weigelt et al. (2015).

104

105 The Zeppelin GAW station is located on the ridge of the Zeppelin Mountain (78°54`N, 11°52`E) at 474 m a.s.l.,
106 about 2 km from Ny Ålesund on the west coast of Spitsbergen which is the largest of the Svalbard Islands.
107 Mercury measurements are described by Aspino et al. (2005).

108



109 Waldhof (52°48'N, 10°45'E) is a rural background site located in the northern German lowlands in a flat
110 terrain, 100 km south-east of Hamburg., The site and analytical method are described in detail by Weigelt et
111 al. (2013).

112

113 Villum Research Station is located at the military outpost Station Nord. It is located in the furthestmost
114 northeastern corner of Greenland on the north–south oriented peninsula of Princess Ingeborg Halvø
115 (81°36' N, 16°40' W), whose northern end is a 20 × 15 km² Arctic lowland plain. The Air Observatory is located
116 2 km south of the central complex of Station Nord that is manned year-round by 5 soldiers. The monitoring
117 site is upwind of the dominant wind direction for Station Nord and thus any effect of local pollution is
118 minimized. Atmospheric measurements at Villum are described in detail by Skov et al. (2004 and 2020).

119

120 Andøya observatory (69.3°N, 16°E) is situated a few hundred meters away from ALOMAR (Arctic Lidar
121 Observatory for Middle Atmosphere Research), which is located at the west coast on a mountain at the island
122 Andøya in Northern Norway. ALOMAR is part of Andøya Space Center. More details about measurements at
123 Andøya are available in Berg et al. (2008).

124

125 Amderma Polar Station is located near the Amderma settlement of the Arkhangelsk Arctic region of Russia
126 near the coast of the Kara Sea (69°43'N, 61°37'E; Yugor Peninsula, Russia). Gaseous mercury has been
127 measured since 2001 until 2017. The site and the mercury measurements are described by Pankratov et al.
128 (2013).

129

130 At all sites mercury was measured using Tekran 2537 instrument (Tekran Inc, Toronto, Canada), an
131 automated dual-channel, single amalgamation, cold vapor atomic fluorescence (CVAFS) analyzer. The
132 instrument has two gold cartridges. While mercury is collected on one of them during the sampling period,
133 the other is being analyzed by thermodesorption and CVAFS detection. The functions of the cartridges are
134 then alternated, allowing for quasi-continuous measurement. The instruments are usually protected by an
135 upstream PTFE filter against dust and aerosols. As discussed by Slemr et al. (2016), gaseous oxidized mercury
136 (GOM) compounds are collected on the gold cartridges and were found to be converted to elemental mercury
137 (GEM) probably during the thermodesorption. The instrument is thus able to measure total gaseous mercury
138 (TGM) provided that GOM compounds reach the cartridges. This is frequently not the case because the GOM
139 compounds are sticky and can thus be removed on the way from the inlet to the cartridges. Soda-lime filter
140 used at Villum is known to capture GOM. Sea salt on the walls of the sampling tubing and on the PTFE filter
141 at coastal stations, such as Mace Head, Andøya, Amderma, and possibly Zeppelin, is also likely to remove
142 GOM. We conclude that GEM is being measured at Mace Head (Weigelt et al., 2015), Villum (Skov et al.,



143 2020), Andøya, Amderma, and Zeppelin (Durnford et al., 2010). With the exception of polar depletion events,
144 GEM is the dominant form of atmospheric mercury, accounting for more than 99% of TGM in marine
145 boundary layer (Soerensen et al., 2010) and more than 95% in the continental one (Lindberg and Stratton,
146 1998). We thus treat all data as TGM.

147

148 • **Back-Trajectory Analysis.**

149

150 To evaluate the spatial coverage and sources of air sampled at the five stations, three dimensional reanalysis
151 air mass back-trajectories were calculated at each site for 120 h, every 12 h, with arrival times at 0:00 and
152 12:00, for all years at an arrival height of 50 m and 500 m above ground using HYSPLIT (v.4.2.0, NOAA) as
153 described by Stein et al. (2015). All individual back-trajectories generated by HYSPLIT were converted to
154 text shape files and imported into R (R Project for Statistical Computing), merged with concentration files
155 and used for spatial analysis. To account for the speed and atmospheric residence time of air masses, each
156 continuous back-trajectory line was transformed into 120 hourly points.

157

158 Concentration-weighted trajectories (CWT), also called field concentration, are a function of average mercury
159 concentrations that were obtained every 12 h and of the residence time of a trajectory in each grid cell. The
160 12-hour trajectory segment endpoints for each back trajectory that corresponds to each 12 h TGM, or GEM,
161 were retained. For a 120-hour trajectory duration, 84 trajectory segment end points were calculated. This
162 transformation of trajectories into hourly segments allowed the subsequent application of a kernel density
163 tool to the combined back-trajectory air mass points from all sampling sites in order to create a density map
164 of the continental concentration and spatial coverage of concentration airflows sampled at the sampling site
165 over the course of an entire year. Seasonal back-trajectory maps were also generated for evaluation of po-
166 tential seasonal changes in the coverage and sources of airflows (with seasons defined as summer (June, July,
167 and August), autumn (September, October, and November), winter (December, January, and February), and
168 spring (March, April, and May).

169 • **Concentration-weighted trajectories (CWT) and probability mass function (PMF) models**

170

171 The source apportionment for Mace Head was performed based on the mass conservation principle with the
172 inclusion of potential rotated infinity matrices transformation producing factors with chemical profile signed
173 by tracer species linked to its source. The full description of PMF and its reconstruction consideration,
174 chemical species considered, uncertainties, and constraining of factors are presented in Custodio et al.
175 (2020).

176



177 The CWT is an approach which can be used to indicate the probability of a grid cells contribution to pollution
178 events (Cheng et al. 2013). It is based on a statistical model and can incorporate meteorological information
179 in its analysis scheme to identify the average concentration in areas for pollutants based on a conditional
180 probability that an air parcel that passed through a cell with a gradient concentration displays a high
181 concentration at the trajectory endpoint (Ashbaugh et al. 1985, Byčenkienė, et al. 2014). In this study, the
182 assessment was performed on annual bases, the concentrations in grid cells were calculated by counting the
183 average concentration of trajectory segment end points that terminate within each cell as described by
184 Byčenkienė, et al. (2014) and Tang et al. (2018).

185

186 **3 Results and discussion**

187

188 In this section, we present the time series and trend of TGM, or GEM, concentrations from a data set
189 composed of 8736 days, 4888 days, 6650 days, 5188 days, 4123 days, and 7580 days of measurements
190 covering the period from November 1995 to December 2019 (Mace Head), June 2001-March 2017
191 (Amderma), January 2000 to 2019 (Zeppelin), January 2006 to December 2019 (Waldhof), from January 2010
192 to December 2016 (Andøya), and from June 1999 to December 2019 (Villum) respectively. The data are
193 summarized in in Figure 1.

194 TGM concentrations and their frequency distributions shown in Figure 1 display distinct differences between
195 the stations. TGM concentrations at Villum, Amderma, and Zeppelin decrease frequently to values near zero
196 (minima of 0.0, 0.0, and 0.1 ng m⁻³ at Villum, Amderma, and Zeppelin, respectively) and their frequency
197 distribution is skewed to lower values as documented by differences between the lower average than median
198 TGM concentrations and the lowest 5th percentiles of all sites with 0.55, 0.62, and 1.04 ng m⁻³ at Villum,
199 Amderma, and Zeppelin, respectively. The seasonal occurrence of the polar depletion events at these three
200 stations is characteristic for the Arctic sites with ice and snow coverage (Steffen et al., 2008). The TGM
201 frequency distribution at Zeppelin is less skewed than at Villum and Amderma perhaps because of the
202 Zeppelin altitude of almost 500 m asl, which is above the layer with most intensive halogen chemistry within
203 the first 100 – 200 m above snow (Tackett et al., 2007).

204 The distribution of TGM concentrations at Waldhof, a mid-latitude station in Central Europe, is on the
205 contrary skewed to higher values because of frequent events with local and regional pollution (Weigelt et al.,
206 2013). The average and median TGM concentrations are the highest of all the investigated stations, and the
207 average is substantially higher than median.

208 The frequency distribution at Andøya is nearly symmetric, neither skewed to low nor to high TGM
209 concentrations although a pronounced seasonal variation can be observed. At latitude comparable to that of
210 Amderma there are no pronounced depletion events at Andøya because it is exposed to Gulf stream and as
211 such free of ice for most of the year. Events with local and regional pollution are also missing at Andøya. TGM



212 frequency distribution at Mace Head is similar to that at Andøya and the average and median TGM
213 concentrations are nearly the same as both stations are exposed to air originating mostly from the Atlantic
214 Ocean. Opposite to Andøya, TGM frequency distribution is slightly skewed to higher concentration because
215 of the local pollution and occasional air transport from Europe (Weigelt et al., 2015).

216

217 3.1 Seasonal variation

218 Figure 2 shows that the seasonal variations are similar at Mace Head, Waldhof, and Andøya with the
219 maximum TGM concentrations in late winter and early spring, the minimum in late summer and early
220 autumn. Similar seasonal variation has been observed at most of the mid-latitude sites in the northern
221 hemisphere (e.g. Cole et al., 2014; Weigelt et al., 2015; Sprovieri et al., 2016). It is usually accompanied by a
222 summer maximum in wet deposition (Gratz et al., 2009; Prestbo and Gay, 2009; Zhang and Jaeglé, 2013;
223 Sprovieri et al., 2017) which is caused by stronger oxidation of Hg^0 to Hg^{2+} in summer providing more Hg^{2+} for
224 scavenging by rain (Holmes et al., 2010; Zhang et al., 2012; Zhang and Jaeglé, 2013; Horowitz et al., 2017).
225 GEM uptake by vegetation can also contribute to summer minimum of TGM concentrations at midlatitudes
226 (Jiskra et al., 2018).

227 Seasonal variations in mercury at Amderma, Villum and Zeppelin are influenced by polar depletion events in
228 spring and the subsequent reemission of the deposited mercury from snow in summer which result in
229 pronounced TGM minima in April and May and maxima in July (Steffen et al., 2008, 2015; Dommergue et al.,
230 2010; Cole and Steffen, 2010; Cole et al. 2014; Skov et al. 2020). A similar pattern is also observed at Alert
231 (Cole et al. 2014). Note the larger amplitude of seasonal variation at Arctic stations ($0.8 - 1.2 \text{ ng m}^{-3}$) when
232 compared to the mid-latitude ones ($0.95 - 1.07 \text{ ng m}^{-3}$). Zeppelin has a substantially smaller amplitude of
233 seasonal variation than Amderma and Villum, probably because of its altitude as already noted in the
234 discussion of the frequency distributions. Andøya, although located at a comparable latitude as Amderma, is
235 only slightly influenced by the polar depletion events because it is ice-free for most of the year, as already
236 mentioned.

237 Figure 2 shows density maps which are based on the seasonal mean mercury concentration associated with
238 respective trajectories which arrived synchronously at all six stations. The northern parts of the spring and
239 summer panels show over the Arctic Ocean the lowest and highest mercury concentrations, respectively,
240 which is consistent with the spring polar mercury depletion and summer emission of the mercury deposited
241 during the depletion events. The highest TGM concentrations over the middle of the North Atlantic occur in
242 winter, the lowest ones in summer and autumn which is consistent with the seasonal variations at Mace Head
243 and Andøya. High TGM levels over large part of the Europe occur in all seasons. The highest concentrations
244 by level and extension occur in winter and spring, somewhat lower in summer and autumn.

245



246 3.2 Temporal trends and regional source of TGM

247

248 Figures 3 and 1S show the Kernel-regression of mercury concentrations at Mace Head, Amderma, Andøya,
249 Villum, Waldhof, and Zeppelin. Both figures show a non-monotonic concentration change with temporary
250 increases to intermediate maxima at Waldhof, Zeppelin, and most pronounced at Villum with a maximum in
251 2013. The overall trend of GEM concentrations at all sites points in downward direction. Table 1 summarizes
252 the overall trends calculated by LSQF from monthly medians and compares them with those at Mace Head
253 over the same periods of available measurements. Averages of monthly medians over the same periods are
254 also listed. Mace Head was taken as a bench mark because of the longest and most complete data record. In
255 addition, the trend at Mace Head represents the baseline trend (Weigelt et al., 2015). All trends in the table
256 are significant at >99.9% level as are the differences between the trends at the sites and those at Mace Head.
257 TGM concentration at Mace Head decreased with an annual rate of $-0.0244 \pm 0.0011 \text{ ng m}^{-3} \text{ yr}^{-1}$ in 25 years
258 ($-0.0256 \pm 0.0012 \text{ ng m}^{-3} \text{ yr}^{-1}$ in 24 years). For different periods within these long-term measurements, the
259 decrease rate at Mace Head varied between -0.0244 and $-0.0346 \text{ ng m}^{-3} \text{ yr}^{-1}$ as illustrated by Figure 3. The
260 average TGM concentrations at Waldhof are substantially higher than those at Mace Head demonstrating
261 the continuing presence of regional emissions. The downward trend at Andøya is comparable to that at
262 Waldhof but substantially smaller than at Mace Head for the period of Andøya measurements. The average
263 TGM concentration at Andøya is somewhat higher than at Mace Head.

264 Of the Arctic stations, TGM concentration at Zeppelin decreased with only $-0.0087 \text{ ng m}^{-3} \text{ yr}^{-1}$ when compared
265 to $-0.279 \text{ ng m}^{-3} \text{ yr}^{-1}$ for the same period at Mace Head. Cole et al. (2013) have reported a trend of $+0.002 \text{ ng}$
266 $\text{m}^{-3} \text{ yr}^{-1}$ (-0.007 to $+0.012 \text{ ng m}^{-3} \text{ yr}^{-1}$, 95% confidence range) for Zeppelin in the decade 2000 – 2009 which is
267 consistent with the trend value presented here for 2000 – 2019. The average TGM concentration of $1.57 \pm$
268 0.24 ng m^{-3} for the decade 2000 – 2009 (Cole et al., 2013) is almost identical with $1.55 \pm 0.14 \text{ ng m}^{-3}$ reported
269 here for the years 2000 – 2019, too. A somewhat higher but comparable decrease rate of $-0.012 \text{ ng m}^{-3} \text{ yr}^{-1}$
270 (-0.021 to $0.000 \text{ ng m}^{-3} \text{ yr}^{-1}$, 95% confidence interval) was reported for Alert for the 2000 to 2009 period (Cole
271 et al., 2013). The average TGM concentration of $1.50 \pm 0.35 \text{ ng m}^{-3}$ at Alert is also comparable to that of
272 Zeppelin in the 2000 – 2009 period (Cole et al., 2013). Figure 3 shows at Zeppelin a broad maximum around
273 2006.

274 Based on LSQF the TGM at the Arctic stations Amderma and Villum behave differently. The downward trends
275 of -0.0327 ± 0.0047 and $-0.0409 \pm 0.0072 \text{ ng m}^{-3} \text{ yr}^{-1}$ at Amderma and Villum, respectively, are roughly
276 comparable and both are substantially larger than those at Mace Head for the respective periods. Their trend
277 uncertainties are substantially larger than the uncertainties at the other stations. On the other side, the
278 average TGM concentrations at Amderma and Villum are comparable to those at Mace Head for the
279 respective periods, albeit with substantially higher standard deviations. This is partly due to the short periods
280 with varying trend at Amderma and even a pronounced temporal maximum at Villum.



281 The higher level of atmospheric mercury at Villum in 2013 is consistent with an elevated mercury level over
282 Greenland in that year, as deduced from backward trajectory analyses shown in Figure 4. Large subglacial
283 source of mercury at Greenland has been recently reported by Hawkings et al. (2021). The increase of GEM
284 at Villum in 2010 and 2013, which drives the trend up during this period, corresponds to two periods of
285 negative extreme at Arctic Oscillation (AO). The extreme on AO and North Atlantic Oscillation (NAO) can
286 enhance the mercury discharge from ice to the atmosphere. Bevis et al. (2019) report an anomalous ice mass
287 loss at Greenland in the 2010-2014 epoch. The abrupt ice melting was driven mainly by changes in air
288 temperature and solar radiation caused by atmospheric circulation anomalies.

289 In addition, the negative phase of the summertime NAO index increases the prevalence of high pressure,
290 clear-sky conditions, enhancing surface absorption of solar radiation and decreasing snowfall, and it causes
291 the advection of warm air from southern latitudes into Greenland. These changes promote higher air tem-
292 peratures, a more extended ablation season and enhanced melt ice (Fettweis et al. 2013). In 2014/2015,
293 when the AO indexes again turned positive and NAO negative, significant ice loss was reestablished (Bevis
294 et al., 2019).

295 The back trajectories of air masses calculated for each site were combined with the measured concentration
296 at a 12h time resolution. The results were used to identify possible regional sources and also to assess
297 temporal variations. Figure 4 shows that calculated air mass back-trajectories for the five monitoring sites
298 mainly reflect air masses transported from the ocean, however, they also indicated elevated concentrations
299 in continental trajectories such as from central Europe which are due to anthropogenic emission sources.
300 Despite a shift to the south that can be associated with uncertainties in the Lagrangian approach, the airflow
301 patterns and concentrations hotspot were consistent with the current knowledge of geolocation of TGM
302 sources in Europe. Figure 4 also shows a high level of mercury associated with air masses coming from the
303 northwest (Canada and Greenland) during the 1997-2000 epoch, 2005, 2010, 2014 besides of 2013 already
304 mentioned.

305 The most revealing detail in the observed trend of TGM is displayed in Figure 4, where it is noticeable that
306 the downward trend is ongoing on a regional scale. This decrease could represent a change in the balance
307 between sources and sinks of mercury in the atmosphere.

308 The downward trend seems to be driven by decreasing concentrations in continental Europe. This phenom-
309 enon is observed mainly after 2005 when data from Waldhof is considered. The downward trend in mercury
310 concentration is observed in all trajectories, even in remote areas, indicated by the yellow fades to green.
311 This phenomenon can be explained only by reductions in global atmospheric mercury sources. In addition,
312 Figure 4 also shows that the decrease is more pronounced in the hotspot areas identified as anthropogenic
313 sources, where the colour shifts from dark to light red in plots from 2005 to 2019.



314 The later downward trend at Zeppelin and Villum (Figure 3, 1S), suggests that these remote, high latitude
315 stations are less affected by direct European continental emission.

316 The seemingly non-monotonic downward trends with inter-annual ups and downs are not well explained.
317 However, an inspection of the Mace Head data (e.g. in Figure 3 and 4) reveal that this trend is composed of
318 two segments: one starting in 1999 and ending approximately in 2010 and a second one in 2014 after a
319 biennial upward tendency. It could be premature to assume that the atmospheric mercury trend can be
320 driven simply by a political decision. However, it can be seen that the two important TGM trend deflections
321 in 1999 and 2014, coincide with COUNCIL DIRECTIVE 1999/31/EC, a European Union (EU) directive that
322 regulates waste management of landfills in the EU and the mercury international treaty (Minamata
323 Convention on Mercury) designed to protect human health and the environment from anthropogenic
324 emissions and releases of mercury approved on 10 October, 2013. Continental and international
325 environmental treaties are the result of long political and societal debate and commitment to such deal could
326 reflect an already established control policy at the national level.

327 For example, in 1990 The United States Clean Air Act, put mercury on a list of toxic pollutants that needed to
328 be controlled to the greatest possible extent, forcing industries that release high concentrations of mercury
329 into the environment to install maximum achievable control technologies (MACT). In 2005, the EPA
330 promulgated a regulation that added power plants to the list of sources that should be controlled and
331 instituted in the nation, and in 2011 new rules for coal-fired power plants were announced by EPA (*State of
332 new Jersey, et al. 2008, Castro Mark S., Sherwell John 2015*).

333 Additionally, in 2007 the European Union implemented new mercury control measures, banning mercury in
334 new non-electrical measuring devices, such as thermometers and barometers (*Jones, H. 2007*).

335 We note that Waldhof, a continental station close to anthropogenic sources in Europe, corroborates the
336 interpretation of an anthropogenic emission driven mercury trend. This station shows a more pronounced
337 TGM decrease between 2005-2010 compared to the years since then. Zhang et al. (2016) presented a revised
338 inventory of Hg emissions for the estimation of artisanal and small-scale gold mining emissions, and,
339 accounting for the change in $\text{Hg}^0/\text{Hg}^{\text{II}}$ speciation of emissions from coal-fired utilities after implementation of
340 emission controls targeted at SO_2 and NO_x , those authors estimate a factor of 20% decrease in atmospheric
341 emission from 1990 to 2010. Natural sources can contribute up to 40% of the atmospheric mercury budget
342 (*Pirrone, et al., 2010*); however, a trend on such a source is not observed or reported in the literature, so far.

343

344 **3.3 Probability of source contribution.**

345 Based on the TGM associated with each air mass trajectory, we investigated the impact of atmospheric cir-
346 culation on continental Europe and Northern Atlantic Ocean and observe distinct concentration patterns for
347 the ocean and continental regions. We observed for example, that air masses arriving at Mace Head from



348 central Europe show distinct trends. We compared the regional patterns of TGM with other pollutants (CO,
349 CO₂, CH₄, O₃, CHCl₃, CCl₄, and CFCs) also measured at Mace Head and find that TGM shows a similar pattern
350 concerning source location as the other species closely related to anthropogenic sources. However, TGM
351 displays a downward trend, with decreasing concentrations in air masses from central Europe and England.
352 Figure 4 shows the concentration- weighted trajectory maps for TGM measurements over Mace Head,
353 Amderma, Andøya, Villum, Waldhof and Zeppelin. It can be seen that the highest concentrations are almost
354 exclusively from air masses over central Europe. Exceptions are 1997 to 2000 which indicate high levels of
355 TGM in air masses coming from Northwest. However, it should be mentioned that CWT for this period
356 computed only Mace Head data and Villum (1999-2000).

357 The results also show a lower level of TGM in air masses segments over the North Atlantic region. This region
358 is constantly associated with a sink of anthropogenic pollutants.

359 Based on our analysis so far, our hypothesis is that the mercury concentration in North Atlantic air masses is
360 affected by the intensity of transport from important regional and global sources and also by temporal
361 changes in these sources. For example, the high mercury concentrations observed in the late 1990's coincide
362 with higher contributions from continental air masses. During 2001, a noticeable reduction in the Mace Head
363 TGM concentration was observed, corresponding to a lesser influence of continental European air masses.
364 This was due not only to a lower frequency of air masses from continental Europe but also lower concentra-
365 tion of TGM in those air masses compared to previous years. A similar phenomenon was observed in the
366 trend during 2005/2006 and 2008 to 2010 when an increase and decrease of inter-annual trend corresponded
367 to higher and lower CWT in air masses coming from continental Europe (Figure 2S).

368 In a five-year source apportionment of mercury at Mace Head, Custodio et al. (2020) show that a factor with
369 high load of anthropogenic species could explain downward trends of TGM. The downward trend of that
370 factor was associated with a reduction in emissions due to cleaner manufacturing processes involving
371 mercury and regulations limiting the emissions from coal-fired power plants since the 1980s, as well as a
372 reduction in the release of mercury from commercial products since 1990s (Streets et al. 2011, Zhang et al.,
373 2016).

374 Here we extend the source apportionment analysis back to 1996. The extended reconstruction of the main
375 sources of mercury back to 1996, shown in Figure 5, displays a similar apportionment pattern to that reported
376 by Custodio et al. (2020). The source apportionment indicates a baseline factor characterized by high load of
377 anthropogenic species accounting for 65% of TGM mass. The baseline factor has already been proposed as
378 the driving factor for mercury trends at Mace Head by Custodio et al. (2020). In this study, this factor displays
379 a downward trend of 2.7 % yr⁻¹, and correlates (r =0.97) with the mercury trend (Figure 6). A factor with load
380 of anthropogenic species driving the Mace Head TGM trend down by a strength of 97 % at the level of 0.001



381 (p-values) is also supported by Figure 4, which displays a temporal decrease in mercury level in reanalysis
382 backward trajectory.

383 One important consideration to take into account is that the baseline factor is interpreted as global mercury
384 budget from several sources which were not solved by PMF, such factor could also take into account the
385 strength of non-modulated extremes events or periodic oscillations such as ENSO as speculated by Slemr et
386 al. (2020) and references therein, those events can be a reason for increase rotation in the mercury trend,
387 imposing significance and raising the correlation.

388 The Global Mercury Assessment inventory (AMAP/UNEP, 2019) estimates a contribution of combustion
389 sources to atmospheric mercury at 24%. In this study the combustion factor, which was indicated by high
390 load of CO, accounted for 20% of total TGM mass at Mace Head (Figure 5). A slight decreasing trend was
391 observed in this factor, which could be associated with the implementation of emission controls on coal-fired
392 utilities as proposed by Zhang et al. (2016) in a revised inventory of Hg emissions.

393 However, as reported by Custodio et al. (2020) this trend should be taken with caution since the combustion
394 factor was fingerprinted by CO, a short-lived species (1-3 months) with significant seasonal and atmospheric
395 transport dependence.

396 The ocean factors account for 12% of total TGM mass at Mace Head and was identified by a high load of CHCl₃
397 (Figure 5). CHCl₃ used to trace sign ocean factor, is a trace atmospheric gas originating 90% from a natural
398 source, being offshore seawater the largest issuer (McCulloch, 2003).

399 As reported by Custodio et al. (2020) and references therein, the residence time of mercury in the ocean is
400 substantially longer than in the atmosphere, ranging from years to decades or millennia. Human activity has
401 substantially increased the oceanic mercury reservoir and consequently is affecting the fluxes of mercury
402 between the sea and atmosphere (Strode et al., 2007).

403 The acidification of oceans, climate change, excess nutrient inputs, and pollution are fundamentally changing
404 the ocean's biogeochemistry (Doney, 2010) and will certainly also influence mercury ocean-air fluxes in a still
405 unknown direction.

406 This study shows an upward trend in the oceanic factor after 2010, as can be seen in Figure (5), however its
407 significance, implication and causes remain to be determined.

408

409 **4 Conclusion**

410 A conundrum in the observed negative trend in mercury in Europe and Northern Atlantic over the past two
411 decades is explained in this study by a decrease in anthropogenic emissions. The significant decline in con-
412 centrations of TGM over the past two decades demonstrates that regulatory measures across Europe have
413 been successful in reducing the atmospheric concentration of this species although an extensive fossil fuel
414 use and a legacy of stockpiles in the environment continue to pose a challenge.



415 These results show the transport pattern of atmospheric mercury and reveal that a baseline factor with a
416 high load of long-lived anthropogenic species dominates the source of mercury in the Northern Atlantic and
417 highlight the need for continued monitoring of the TGM and its sources. This study brings a monitoring con-
418 cept for mercury on a continental scale which can be extended to a Global Monitoring plan by integration of
419 the mercury monitoring network, potentially identifying hotspot concentration areas and their change over
420 time.

421 This large-scale, long-term trend data evaluation can be used for assessing the effectiveness of the Minamata
422 Convention.

423 More specific conclusions include the following:

- 424 ➤ Enhancement of mercury in the air masses over Greenland in summer during epochs of atmospheric
425 circulation anomalies.
- 426 ➤ Mercury downward trends of $2 \pm 3\% \text{ yr}^{-1}$, $2.1 \pm 1.5\% \text{ yr}^{-1}$, $1.6 \pm 3.9\% \text{ yr}^{-1}$, $4 \pm 16\% \text{ yr}^{-1}$, $2 \pm 4\% \text{ yr}^{-1}$,
427 and $3 \pm 3\% \text{ yr}^{-1}$ at Amaderma, Andøya, Mace Head, Villum, Waldhof and Zeppelin respectively are
428 influenced by regional sources and then biased for global trend.
- 429 ➤ The observed TGM downward trend at Northern Atlantic and Arctic seems to be driven by
430 decreasing in concentration in continental Europe.
- 431 ➤ A baseline factor with high load of anthropogenic species drives the mercury trend down by a
432 strength of 97 % at the level of 0.001 (p-values) based on source reconstruction at Mace Head.
- 433 ➤ Combustion sources could account for 20 % of TGM with a slightly decreasing trend, and ocean
434 sources account for 12 % with a slightly increasing trend.

435

436 **Authors Contribution:**

437 **DC** proposed the article, processed data and wrote the article. **FS** advised the article strategy, calculate the LSQF and reworded the
438 experimental description and section 3.1. **KAP** provided data and evaluated the findings. **TGS** provided data, support the writing and
439 discussions. **FFP** provided data and participate in the discussion. **IS** supported the calculation in scripts, data assimilation, besides
440 provide meteorological and Lagrangian analysis. **KP** supported the trajectories calculation and discussion. **HS** provided data and dis-
441 cussion in its interpretation. **JB** and **RE** endorse and supported the article preparation, respectively.

442

443

444 Table 1: Comparison of TGM trends and average concentrations at Zeppelin, Waldhof, Andøya, Amderma, and Villum
445 with those at Mace Head. The trends were calculated by the least square fit (LSQF) of monthly medians over the same
446 months for which the measurements are available. Average TGM concentrations were calculated as average of monthly
447 medians over months with synchronous measurements.

448

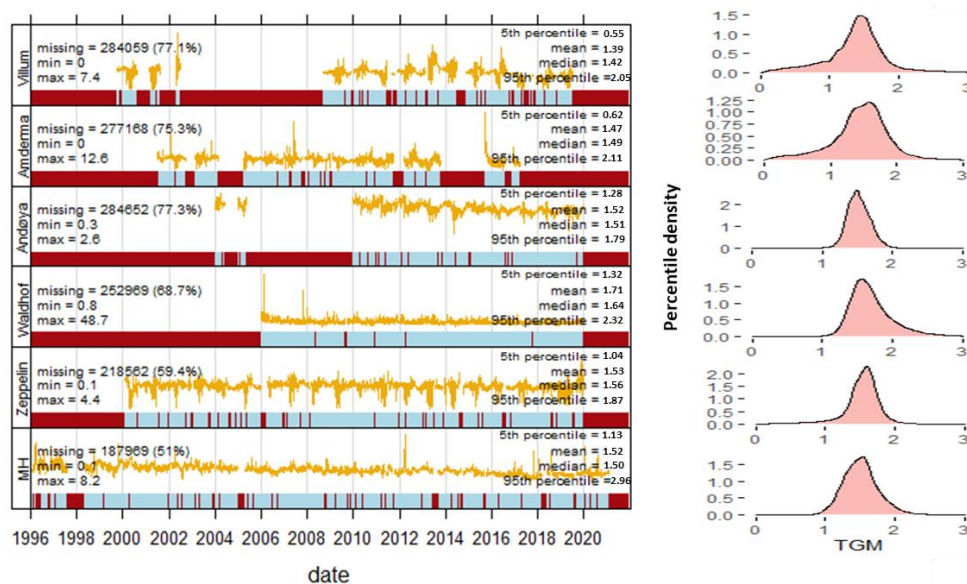
| Site | Period, number of months | Trend [$\text{ng m}^{-3} \text{ yr}^{-1}$] | | TGM average concentration [ng m^{-3}] | |
|-----------|--------------------------|--|----------------------|--|-------------------|
| | | Site | Mace Head | Site | Mace Head |
| Mace Head | Feb 1996 – Dec 2020, 279 | | -0.0244 ± 0.0011 | | |
| Mace Head | Feb 1996 – Dec 2019, 267 | | -0.0256 ± 0.0012 | | |
| Zeppelin | Feb 2000 – Dec 2019, 222 | -0.0087 ± 0.0015 | -0.0279 ± 0.0013 | 1.548 ± 0.141 | 1.483 ± 0.196 |



| | | | | | |
|---------|-----------------------------|----------------|------------------|-------------|-------------|
| Waldhof | Jan 2006 – Dec 2019, 161 | -0.0243±0.0025 | -0.0280 ± 0.0022 | 1.649±0.161 | 1.399±0.158 |
| Andøya | Jan 2004 – Dec 2019, 119 | -0.0262±0.0023 | -0.0346 ± 0.0029 | 1.519±0.127 | 1.368±0.165 |
| Amderma | Jul 2001 – Mar 2017, 133 | -0.0327±0.0047 | -0.0257 ± 0.0022 | 1.480±0.265 | 1.517±0.153 |
| Villum | Sep 2008 – Jun 2019, 111 | -0.0409±0.0072 | -0.0293 ± 0.0031 | 1.372±0.274 | 1.371±0.140 |

449

450

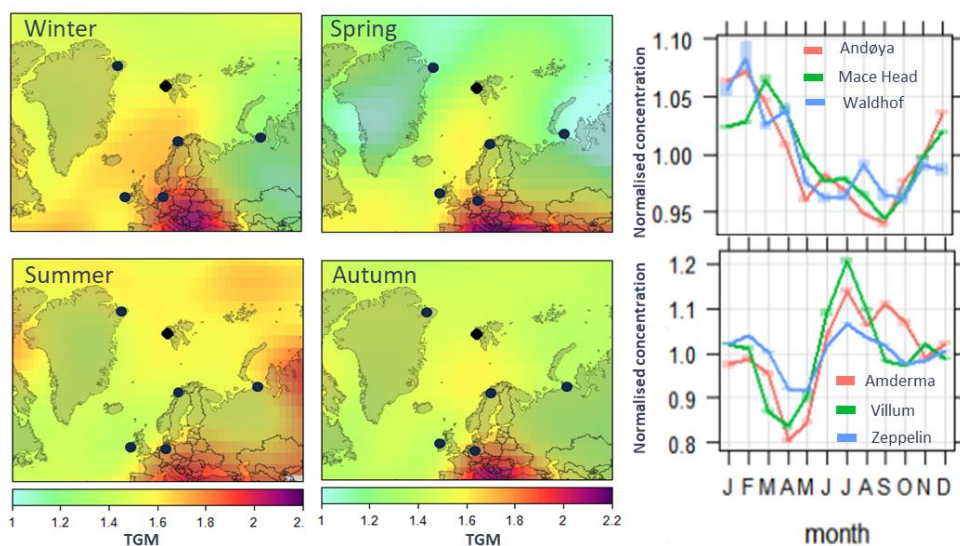


451

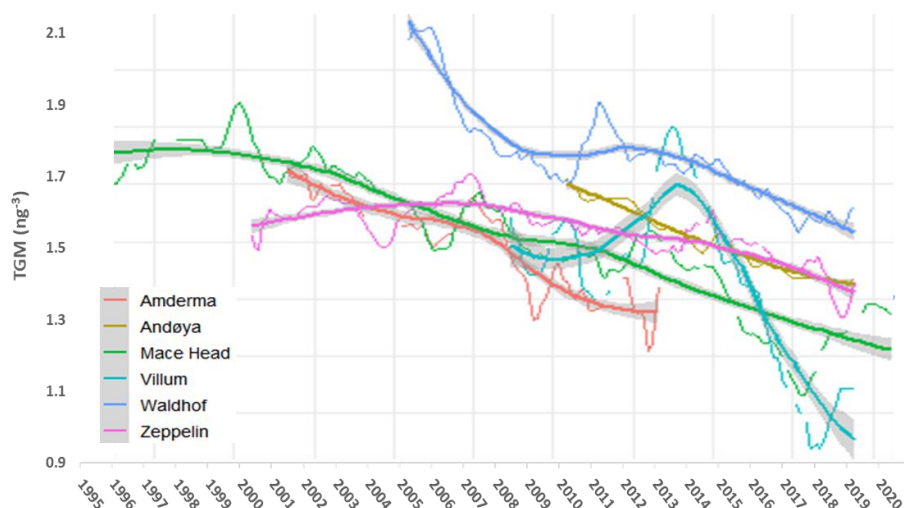
452 Figure 1: Summary of time series of TGM (ng m^{-3}) measured at Mace Head, Zeppelin, Waldhof, Andøya,
 453 Amderma and Villum on the left side. Distributions density of the measured concentrations on the left side.

454 *The red and blue bars on the time axis represent the missing and available data periods, respectively.

455



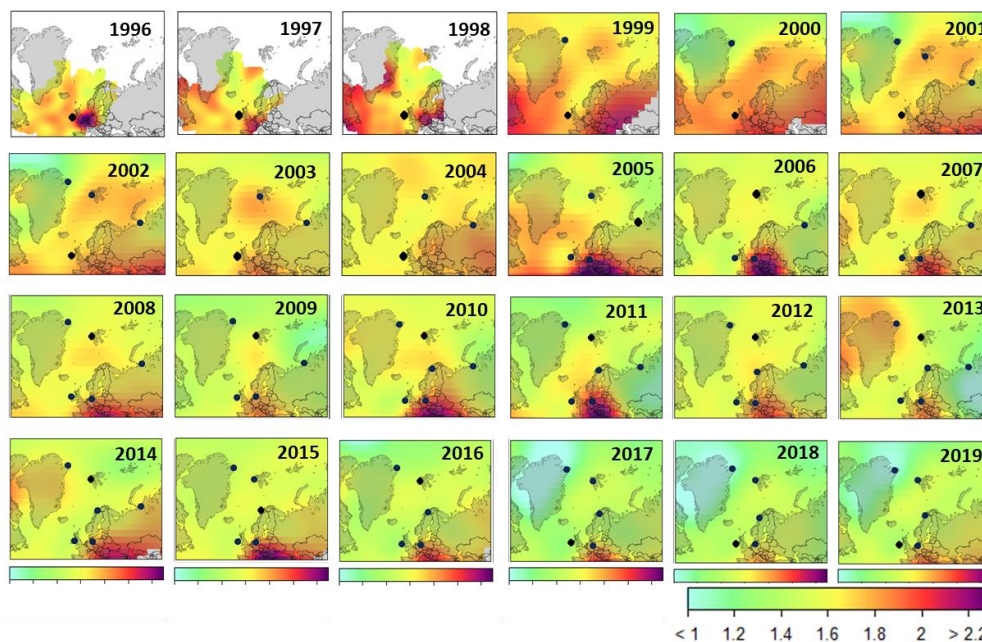
456
 457 Figure 2: Left panels: The density map of atmospheric mercury concentrations in different seasons. Right panels:
 458 Normalized annual variation of the mercury concentrations at Arctic stations (Amderma, Villum, Zeppelin) and at the
 459 mid-latitude ones (Mace Head, Waldhof, and Andøya). The shaded areas are the 95% confidence intervals for the
 460 monthly mean.
 461



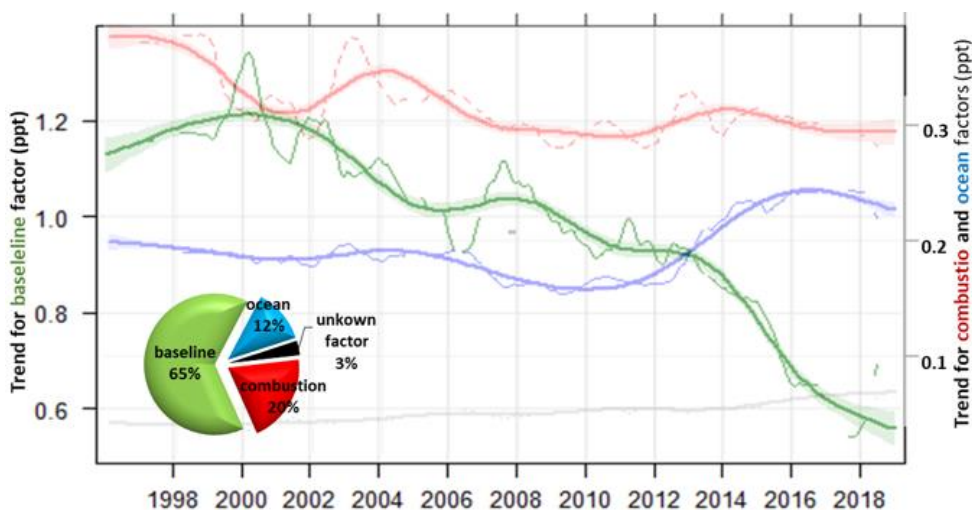
462
 463 Figure 3. Kernel-regression of TGM at Amderma, Andøya, Mace Head, Villum (GEM), Waldhof, and Zeppelin for the
 464 period of 2001-2013, 2010-2019, 1995-2019, 2008-2019, 2006-2019, and 2000-2019 respectively. The smooth lines and
 465 shaded areas represent the Kernel-regression at 95% significance level. The thin lines show the monthly time series of
 466 TGM after removing annual cycles with amplitudes of 0.49 ng m⁻³, 0.23 ng m⁻³, 0.17 ng m⁻³, 0.30 ng m⁻³, 22 ng m⁻³, and
 467 0.25 ng m⁻³ respectively for Amderma, Andøya, Mace Head, Villum, Waldhof, and Zeppelin. The annual cycle was



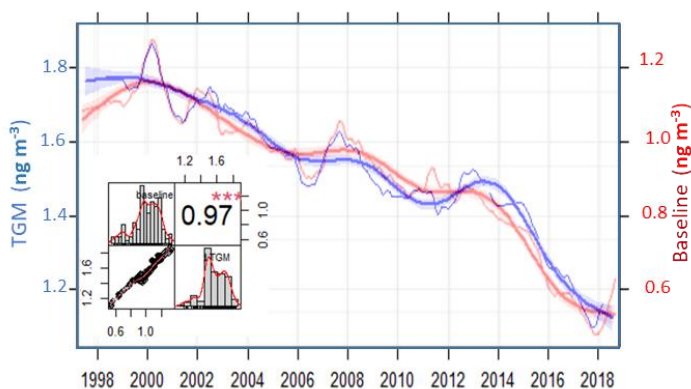
468 calculated based on seasonality of the time series decomposition. *An individual plot regression for each station is
469 presented in Figure 1S.
470
471
472



473
474 Figure 4: Concentration level (concentration-weighted trajectory) of TGM (ng m^{-3}) based on the mercury concentration
475 associated to its reanalysis backward trajectory at Amderma, Andøya, Mace Head, Villum, Waldhof, and Zeppelin. *The
476 black dots show the arriving point (stations) considered for each year.
477
478
479



480
481 Figure
482 5: Time series (thin lines) and percentile average contribution (pie) of factors solved by PMF in the TGM reconstruction
483 for Mace Head from 1996 to 2019, baseline (green) combustion (red), ocean (blue) and unknown factor (grey). The
484 smooth lines and shaded areas represent the Kernel-regression at 95% significance level. The thin lines show the monthly
485 time series with annual cycles removed.



486 Figure 6: Downward trend of TGM (blue) and baseline factor (red) at Mace Head. The smooth lines and
487 shaded areas represent the Kernel-regression and 95% significance level. The thin lines show the monthly
488 time series with annual cycles removed. On the bottom right it is presented the correlation regression with
489 the distribution of each variable and the value of the correlation plus the significance level as stars. p-values
(0.001) <=> symbols(“***”).

490 References

491 AMAP/UNEP: Technical background report for the Global Mercury Assessment 2018, Arctic Monitoring and Assessment
492 Programme, Oslo, Norway/UNEP Chemicals and Health Branch, Geneva, Switzerland, ISBN 978-82-7971-108-7, 2019.



- 493 Ashbaugh, L. L., Malm, W. C. and W. Z. Sadeh, "A residence time probability analysis of sulfur concentrations at Grand
494 Canyon National Park," *Atmospheric Environment Part A*, vol. 19, no. 8, pp. 1263–1270, 1985.
- 495 Aspö, K., Gauchard, P.-A., Steffen, A., Temme, C., Berg, T., Bahlmann, E., Banic, C., Dommergue, A., Ebinghaus, R.,
496 Ferrari, C., Pirrone, N., Sprovieri, F., and Wibetoe, G.: Measurements of atmospheric mercury species during an
497 international study of mercury depletion events at Ny-Ålesund, Svalbard, spring 2003. How reproducible are our
498 present methods?, *Atmos. Environ.*, 39, 7607–7619, 2005.
- 499 Berg, T., Aspö, K., Eiliv Steiness, E., Transport of Hg from Atmospheric mercury depletion events to the mainland of
500 Norway and its possible influence on Hg deposition. *GEOPHYSICAL RESEARCH LETTERS*, VOL. 35, L09802,
501 doi:10.1029/2008GL033586, 2008.
- 502 Bevis, M., Harig, C., Khan, S.A., Brown, A., Simons, F., Willis, M., Fettweis, X., Broek, M.R., Madsen, F.B., Kendrick, E.,
503 Caccamise II, D.J., Dam, T., Knudsen, P., Nylén, T.; Accelerating changes in ice mass within Greenland, and the ice
504 sheet's sensitivity to atmospheric forcing. 1934–1939 | *PNAS* | February 5, 2019 | vol. 116.
505 doi/10.1073/pnas.1806562116.
- 506 Byčenkienė, S., Dudoitis, V., and Ulevičius, V., 2014. The Use of Trajectory Cluster Analysis to Evaluate the Long-Range
507 Transport of Black Carbon Aerosol in the South-Eastern Baltic Region.
- 508 Castro Mark S., *Sherwell John* (2015). "Effectiveness of Emission Controls to Reduce the Atmospheric Concentrations of
509 Mercury". *Environmental Science & Technology*. 49 (24): 14000–14007. Bibcode:2015EnST...4914000C.
510 doi:10.1021/acs.est.5b03576. PMID 26606506.
- 511 Cheng, I., Zhang, L., Blanchard, P., Dalziel, J., and Tordon, R.: Concentration-weighted trajectory approach to identifying
512 potential sources of speciated atmospheric mercury at an urban coastal site in Nova Scotia, Canada, *Atmos. Chem.*
513 *Phys.*, 13, 6031–6048, <https://doi.org/10.5194/acp-13-6031-2013>, 2013.
- 514 Cole, A. S. and Steffen, A.: Trends in long-term gaseous mercury observations in the Arctic and effects of temperature
515 and other atmospheric conditions, *Atmos. Chem. Phys.*, 10, 4661–4672, <https://doi.org/10.5194/acp-10-4661-2010>,
516 2010.
- 517 Cole, A.S., Steffen, A., Pfaffhuber, K.A., Berg, T., Pilote M., Poissant, L., Tordon, R., and Hung, H.: Ten-year trends of
518 atmospheric mercury in the high Arctic compared to Canadian sub-Arctic and mid.latitude sites, *Atmos. Chem. Phys.*,
519 13, 1535–1545, 2013.
- 520 Cole, A.S., Steffen, A., Eckley, C.S., Narayan, J., Pilote, M., Tordon, R., Graydon, J.A., St. Louis, V.L., Xu, X., and Branfireun,
521 B.A.: A survey of mercury in air and precipitation across Canada: patterns and trends, *Atmosphere*, 5, 635–668, 2014.
- 522 Custodio, D., Ebinghaus, R., Spain, T. G., and Bieser, J.: Source apportionment of atmospheric mercury in the remote
523 marine atmosphere: Mace Head GAW station, Irish western coast, *Atmos. Chem. Phys.*, 20, 7929–7939,
524 <https://doi.org/10.5194/acp-20-7929-2020>, 2020.
- 525 Dommergue, A., Larose, C. Fain, X., Clarisse, O., Foucher, D., Hintelmann, H., Schneider, D., and Ferrari, C.P.: Deposition
526 of mercury species in the Ny Alesund area (79°N) and their transfer during snowmelt, *Environ. Sci. Technol.*, 44, 901–
527 907, 2010.
- 528 Doney, S. C.: The growing human footprint on coastal and openocean biogeochemistry, *Science*, 328, 1512–1516, 2010.
- 529 Driscoll, C.T., Mason, R.P., Chan, H.M., Jacob, D.J., and Pirrone, N.: Mercury as a global pollutant: Sources, pathways,
530 and effects, *Environ. Sci. Technol.*, 47, 4967–4983, 2013.
- 531 Durnford, D., Dastoor, A., Figueras-Nieto, D., and Ryjkov, A.: Long range transport of mercury to the Arctic and across
532 Canada, *Atmos. Chem. Phys.*, 10, 6063–6086, 2010.
- 533 EMEP/CCC-Report 3/2020, ISBN 978-82-425-3014-1, Norwegian Institute for Air Research, Kjeller, Norway, 2020.
- 534 EPA, 2005. "Clean Air Mercury Rule". *United States Environmental Protection Agency (EPA)*. Archived from the original
535 on 30 June 2007. Retrieved 1 May 2007.
- 536 Fettweis X, et al. Brief communication "Important role of the mid-tropospheric atmospheric circulation in the recent
537 surface melt increase over the Greenland ice sheet." *Cryosphere* 7:241–248; 2013.
- 538 Gay, D.A., Schmeltz, D., Prestbo, E., Olson, M., Sharac, T., and Tordon, R.: The Atmospheric Mercury Network:
539 measurement and initial examination of an ongoing atmospheric mercury record across North America, *Atmos.*
540 *Chem. Phys.*, 13, 11339–11349, 2013.
- 541 Gratz, L.E., Keeler, G.J., and Miller, E.K.: Long-term relationships between mercury wet deposition and meteorology,
542 *Atmos. Environ.*, 43, 6218–6229, 2009.
- 543 Hawkings, J.R., Linhoff, B.S., Wadham, J.L. et al. Large subglacial source of mercury from the southwestern margin of the
544 Greenland Ice Sheet. *Nat. Geosci.* 2021. <https://doi.org/10.1038/s41561-021-00753-w>
- 545 Holmes, C. D., Jacob, D. J., Corbitt, E. S., Mao, J., Yang, X., Talbot, R., and Slemr, F.: Global atmospheric model for mercury
546 including oxidation by bromine atoms, *Atmos. Chem. Phys.*, 10, 12037–12057, <https://doi.org/10.5194/acp-10-12037-2010>, 2010.
- 547
548 Horowitz, H.M., Jacob, D.J., Amos, H.M., Streets, D.G., and Sunderland, E.M.: Historical mercury releases from
549 commercial products: Global environmental implications, *Environ. Sci. Technol.*, 48, 10242–10250, 2014.



- 550 Horowitz, H. M., Jacob, D. J., Zhang, Y., Dibble, T. S., Slemr, F., Amos, H. M., Schmidt, J. A., Corbitt, E. S., Marais, E. A.,
551 and Sunderland, E. M.: A new mechanism for atmospheric mercury redox chemistry: implications for the global
552 mercury budget, *Atmos. Chem. Phys.*, **17**, 6353–6371, <https://doi.org/10.5194/acp-17-6353-2017>, 2017.
- 553 Jiskra, M., Sonke, J.E., Obrist, D., Bieser, J., Ebinghaus, R., Lund Myhre, C., Pfaffhuber, K.A., Wängberg, I., Kyllönen, K.,
554 Worthy, D., Martin, L.G., Labuschagne, C., Mkololo, T., Ramonet, M., Magand, O., and Dommergue, A.: A vegetation
555 control on seasonal variations in global atmospheric mercury concentrations, *Nature Geosci.*, **11**, 244–250, 2018.
- 556 Jones H. (10 July 2007). "EU bans mercury in barometers, thermometers". *Reuters*. Archived from the original on 3
557 January 2009. Retrieved 12 September 2017.
- 558 Lindberg, S.E., and Stratton, W.J.: Atmospheric mercury speciation: Concentrations and behavior of reactive gaseous
559 mercury in ambient air, *Environ. Sci. Technol.*, **32**,49–57, 1998.
- 560 Marumoto, K., Suzuki, N., Shibata, Y., Takeuchi, A., Takami, A., Fukuzaki, N., Kawamoto, K., Mizohata, A., Kato, S.,
561 Yamamoto, T., Chen, J., Hattori, T., Nagasaka, H., and Saito, M.: Long-term observation of speciated atmospheric
562 mercury during 2007–2018 at Cape Hedo, Okinawa, Japan, *Atmosphere*, **10**, 362, doi:10.3390/atmos10070362, 2019.
- 563 McCulloch, A., Chloroform in the environment: occurrence, sources, sinks and effects. *50*, **10**, 1291–1308; 2003.
564 doi.org/10.1016/S0045-6535(02)00697-5.
- 565 Pankratova, F.F., Konopleva, A.V., Makhurab, A., Katsc, O.V. Analysis of the Data of Long-term Monitoring of
566 Atmospheric Mercury Content and Meteorological Parameters at Amderma Polar Station. ISSN 1068-3739, Russian
567 Meteorology and Hydrology, 2013, Vol. 38, No. 6, pp. 405–413. Allerton Press, Inc., 2013.
- 568 Pirrone N, Cinnirella S, Feng X, et al. Global mercury emissions to the atmosphere from anthropogenic and natural
569 sources. *Atmos Chem Phys*. 2010;10:5951–5964.
- 570 Prestbo, E.M., and Gay, D.A.: Wet deposition of mercury in the U.S. and Canada, 1996 – 2005: Results and analysis of
571 the NADP mercury deposition network (MDN), *Atmos. Environ.* **43**, 4223–4233, 2009.
- 572 Schmeltz, D., Evers, D.C., Driscoll, C.T., Artz, R., Cohen, M., Gay, D., Haeuber, R., Krabbenhoft, D.P., Mason, R., Morris,
573 K., and Wiener, J.G.: MercNet: A national monitoring network to assess responses to changing mercury emissions in
574 the United States, *Ecotoxicology*, **20**, 1713–1725, 2011.
- 575 Skov, H. Christensen, J. Goodsite, M.E. Heidam, N.Z. Jensen, B. Wåhlin, P. and Geernaert, G. (2004) "The fate of elemental
576 mercury in Arctic during atmospheric mercury depletion episodes and the load of atmospheric mercury to Arctic" *ES*
577 *& T.* vol. **38**, 2373–2382.
- 578 Skov, H. Hjorth, J. Nordstrøm, C. Jensen B. Christoffersen C. Poulsen M.B. Liisberg J.B. Beddows, D. Dall'Osto, M.
579 Christensen, J. The variability in Gaseous Elemental Mercury at Villum Research Station, Station Nord in North
580 Greenland from 1999 to 2017 (2020). *ACP*, vol **20**, 13253–13265, doi.org/10.5194/acp-2019-912.
- 581 Slemr, F., Brunke, E.-G., Ebinghaus, R., Temme, C., Munthe, J., Wängberg, I., Schroeder, W., Steffen, A., and Berg, T.:
582 Worldwide trend of atmospheric mercury since 1977, *Geophys. Res. Lett.*, **30**, 1516,
583 <https://doi.org/10.1029/2003GL016954>, 2003.
- 584 Slemr, F., Weigelt, A., Ebinghaus, R., Kock, H.H., Bödewadt, J., Brenninkmeijer, C.A.M., Rauthe-Schöch, A., Weber, S.,
585 Hermann, M., Becker, J., Zahn, A., and Martinsson, B.: Atmospheric mercury measurements onboard the CARIBIC
586 passenger aircraft, *Atmos. Meas. Tech.*, **9**, 2291–2302, 2016.
- 587 Slemr, F., Martin, L., Labuschagne, C., Mkololo, T., Angot, H., Magand, O., Dommergue, A., Garat, P., Ramonet, M., and
588 Bieser, J.: Atmospheric mercury in the Southern Hemisphere – Part 1: Trend and inter-annual variations in
589 atmospheric mercury at Cape Point, South Africa, in 2007–2017, and on Amsterdam Island in 2012–2017, *Atmos.*
590 *Chem. Phys.*, **20**, 7683–7692, <https://doi.org/10.5194/acp-20-7683-2020>, 2020.
- 591 Soerensen, A.L., Skov, H., Jacob, D.J., Soerensen, B.T., and Johnson, M.S.: Global concentrations of gaseous elemental
592 mercury and reactive gaseous mercury in the marine boundary layer, *Environ. Sci. Technol.*, **44**, 7425–7430, 2010.
- 593 Soerensen, A.L., Jacob, D.J., Streets, D.G., Witt, M.L.I., Ebinghaus, R., Mason, R.P., Andersson, M., and Sunderland, E.M.:
594 Multi-decadal decline of mercury in the North Atlantic atmosphere explained by changing subsurface seawater
595 concentrations, *Geophys. Res. Lett.*, **39**, L21810, doi:10.1029/2012GL053736, 2012.
- 596 Sprovieri, F., Pirrone, N., Bencardino, M., D'Amore, F., Carbone, F., Cinnirella, S., Mannarino, V., Landis, M., Ebinghaus,
597 R., Weigelt, A., Brunke, E.-G., Labuschagne, C., Martin, L., Munthe, J., Wängberg, I., Artaxo, P., Morais, F., de Melo
598 Jorge Barbosa, H., Brito, J., Cairns, W., Barbante, C., del Carmen Diéguez, M., Garcia, P.E., Dommergue, A., Angot, H.,
599 Magand, O., Skov, H., Horvat, M., Kotnik, J., Read, K.A., Neves, L.M., Gawlik, B.M., Sena, F., Mashyanov, N., Obolkin,
600 V., Wip, D., Feng, X.B., Zhang, H., Fu, X., Ramachandran, R., Cossa, D., Knoery, J., Maruszczak, M., Nerentorp, M., and
601 Norstrom, C.: Atmospheric mercury concentrations observed at ground-based monitoring sites globally distributed
602 in the framework of the GMOS network, *Atmos. Chem. Phys.*, **16**, 11915–11935, 2016.
- 603 Sprovieri, F., Pirrone, N., Bencardino, M., D'Amore, F., Angot, H., Barbante, C., Brunke, E.-G., Arcega-Gabrera, F., Cairns,
604 W., Comerio, S., del Carmen Diéguez, M., Dommergue, A., Ebinghaus, R., Feng, X.B., Fu, X., Garcia, P.E., Gawlik, P.M.,
605 Hageström, U., Hansson, K., Horvat, M., Kotnik, J., Labuschagne, C., Magand, O., Martin, L., Mashyanov, N., Mkololo,
606 T., Munthe, J., Obolkin, V., Ramirez Islas, M., Sena, F., Somerset, V., Spandow, P., Vardè, M., Walters, C., Wängberg,



- 607 I., Weigelt, A., Yang, X., and Zhang, H.: Five-year records of mercury wet deposition flux at GMOS sites in the Northern
608 and Southern hemispheres, *Atmos. Chem. Phys.*, 17, 2689–2788, 2017.
- 609 Stanley, K. M., Grant, A., O'Doherty, S., Young, D., Manning, A. J., Stavert, A. R., Spain, T. G., Salameh, P. K., Harth, C. M.,
610 Simmonds, P. G., Sturges, W. T., Oram, D. E., and Derwent, R. G.: Greenhouse gas measurements from a UK network
611 of tall towers: technical description and first results, *Atmos. Meas. Tech.*, 11, 1437–1458,
612 <https://doi.org/10.5194/amt-11-1437-2018>, 2018
- 613 *State of New Jersey et al., Petitioners vs. Environmental Protection Agency (Case No. 05-1097) . United States Court of*
614 *Appeals for the District of Columbia Circuit. Argued 6 December 2007, Decided 8 February 2008. Archive from the*
615 *original on 3 February 2011. Retrieved 30 May 2008.*
- 616 Steffen, A., Douglas, T., Amyot, M., Ariya, P., Aspö, K., Berg, T., Bottenheim, J., Brooks, S., Cobbett, F., Dastoor, A.,
617 Dommergue, A., Ebinghaus, R., Ferrari, C., Gardfeldt, K., Goodsite, M.E., Lean, D., Poulain, A.J., Scherz, C., Skov, H.,
618 Sommar, J., and Temme, C: A synthesis of atmospheric mercury depletion event chemistry in the atmosphere and
619 snow, *Atmos. Chem. Phys.*, 8, 1445–1482, 2008.
- 620 Steffen, A., Lehnher, I., Cole, A., Ariya, P., Dastoor, A., Durnford, D., Kirk, J., and Pilote, M.: Atmospheric mercury in the
621 Canadian Arctic. Part 1: A review of recent field measurements, *Sci. Total Environ.*, 509–510, 3–15, 2015.
- 622 Stein, A.F., Draxle, R.R., Rolph, G.D., Stunder, B.J.B., Cohen, M.D., and Ngain, F., (2015). NOAA'S HYSPLIT Atmospheric
623 Transport and Dispersion Modeling System. DOI:10.1175/BAMS-D-14-00110.1.
- 624 Streets, D. G., Devane, M. K., Lu, Z., Bond, T. C., Sunderland, E. M., and Jacob, D. J.: All-time releases of mercury to the
625 atmosphere from human activities, *Environ. Sci. Technol.*, 45, 10485–10491, <https://doi.org/10.1021/es202765m>,
626 2011.
- 627 Strode, S. A., Jaeglé, L., Selin, N. E., Jacob, D. J., Park, R. J., Yantoska, R. M., Mason, R. P., and Slemr, F.: Air-sea exchange
628 in the global mercury cycle, *Global Biogeochem. Cycles* 21, GB1017, doi:10.1029/2006GB002766, 2007.
- 629 Tackett, P.J., Cavender, A., Shepson, P.D., Bottenheim, J.W., Morin S., Deary, J., and Steffen, A.: A study of the vertical
630 scale of halogen chemistry in the Arctic troposphere during polar sunrise at Barrow, AK, *J. Geophys. Res.*, 112,
631 D07306, doi:10.1029/2006JD007785, 2007.
- 632 Tang, Y., Wang, S., Wu, Q., Liu, K., Wang, L., Li, S., Gao, W., Zhang, L., Zheng, H., Li, Z., and Hao, J.: Recent decrease trend
633 of atmospheric mercury concentrations in East China: the influence of anthropogenic emissions, *Atmos. Chem. Phys.*,
634 18, 8279–8291, <https://doi.org/10.5194/acp-18-8279-2018>, 2018.
- 635 Weigelt A, Temme C, Bieber E, Schwerin A, Schuetze M, Ebinghaus R, Kock HH (2013) Measurements of atmospheric
636 mercury species at a German rural background site from 2009 to 2011—methods and results. *Environ Chem* 10:102–
637 110.
- 638 Weigelt, A., Ebinghaus, R., Manning, A.J., Derwent, R.G., Simmonds, P.G., Spain, T.G., Jennings, S.G., and Slemr, F.: Analysis
639 and interpretation of 18 years of mercury observations since 1996 at Mace Head, Ireland, *Atmos. Environ.*, 100, 85–
640 93, 2015.
- 641 Weiss-Penzias, P.S., Gay, D.A., Brigham, M.E., Parsons, M.T., Gustin, M.S., and ter Schure, A.: Trends in mercury wet
642 deposition and mercury air concentrations across the U.S. and Canada, *Sci. Total Environ.*, 568, 546–556, 2016.
- 643 Wu, Q.R., Wang, S.X., Li, G.L., Liang, S., Lin, C.-J., Wang, Y.F., et al.: Temporal trend and spatial distribution of speciated
644 atmospheric mercury emissions in China during 1978–2014. *Environ. Sci. Technol.* 50, 13428–13435, 2016.
- 645 Zhang, Y., and Jaeglé, L.: Decreases in mercury wet deposition over the United States 2004–2010: Roles of domestic and
646 global background emission reductions, *Atmosphere*, 4, 113–131, 2013.
- 647 Zhang, Y., Jaeglé, L., van Donkelaar, A., Martin, R.V., Holmes, C.D., Amos, H.M., Wang, Q., Talbot, R., Artz, R., Brooks, S.,
648 Luke, W., Holsen, T.M., Felton, D., Miller, E.K., Perry, K.D., Schmeltz, D., Steffen, A., Tordon, R., Weiss-Penzias, P., and
649 Zsolway, R.: Nested-grid simulation of mercury over North America, *Atmos. Chem. Phys.*, 12, 6095–6111, 2012.
- 650 Zhang, Y.; Jacob, D. J.; Horowitz, H. M.; Chen, L.; Amos, H.M.; Krabbenhoft, D. P.; Slemr, F.; St. Louis, V. L.; Sunderland,
651 E. M. Observed decrease in atmospheric mercury explained by global decline in anthropogenic emissions. *Proc. Natl.*
652 *Acad. Sci. U. S. A.*, 113,526–531, 2016.